

Analytical Methods

Accepted Manuscript



This is an *Accepted Manuscript*, which has been through the Royal Society of Chemistry peer review process and has been accepted for publication.

Accepted Manuscripts are published online shortly after acceptance, before technical editing, formatting and proof reading. Using this free service, authors can make their results available to the community, in citable form, before we publish the edited article. We will replace this *Accepted Manuscript* with the edited and formatted *Advance Article* as soon as it is available.

You can find more information about *Accepted Manuscripts* in the [Information for Authors](#).

Please note that technical editing may introduce minor changes to the text and/or graphics, which may alter content. The journal's standard [Terms & Conditions](#) and the [Ethical guidelines](#) still apply. In no event shall the Royal Society of Chemistry be held responsible for any errors or omissions in this *Accepted Manuscript* or any consequences arising from the use of any information it contains.

Noninvasive imaging of embryonic stem cell cultures by multiphoton microscopy reveals significance of collagen hydrogel preparation parameters

Xuye Lang,¹ Matthew Spousta,² Yu Jer Hwang³ and Julia G. Lyubovitsky^{1,3,4*}

1. Biochemistry Department, UC Riverside, CA 92521.
2. Cell Biology and Neuroscience, UC Riverside, CA 92521.
3. Cell Molecular and Developmental Biology Program, UC Riverside 92521.
4. Department of Bioengineering, MSE 239 Material Science and Engineering, 900 University Ave. Riverside, CA 92521; Phone (951) 827-7231; Email: julial@ucr.edu

*Corresponding author

Abstract

In situ multiphoton microscopy (MPM) imaging method combining two-photon fluorescence (TPF) and second harmonic generation (SHG) optical signals helped to discover localized disaggregation and restructuring of collagen fibers within 3D hydrogels as a result of stem cell culture. We prepared hydrogels at different solid content (2 g/l or 4 g/l) and self-assembly temperatures (27 °C or 37 °C). In a separate experiment, we stabilized 2 g/l 37 °C hydrogels with the nontoxic cross-linkers carbodiimide (EDC), EDC/*N*-Hydroxysuccinimide (NHS) or genipin. We characterized all collagen hydrogels nondestructively with MPM with and without culturing embryonic stem cells on/within them. We used rheology measurements to assess the flow behavior of the materials we prepared. All cross-linkers reduced the viscous part G'' of the modulus, implying that cross-linked materials are more rigid and non-flowing compared to non-cross-linked hydrogels.

We evaluated nine possible scenarios of how embryonic stem cells could be set up to interact with collagen scaffolds when used in tissue engineering or regenerative medicine applications. The cells encapsulated or placed on top of 4 g/l self-assembled hydrogels extended significantly slower compared to cells interfaced with 2 g/l materials. Cultured cells modified the structure within non-cross-linked materials while the structure within cross-linked hydrogels was less affected. The non-invasive *in situ* MPM imaging analysis in this study is valuable because it enables longitudinal, 3D analysis of structural and functional status of thick, opaque scaffolds as they interact with stem cells and are being degraded.

Keywords: embryonic stem cells, cross-linking, collagen hydrogels, multi-photon imaging

Introduction

The **many** potentialities of employing embryonic stem cells in regenerative medicine, and as models are described in literature.¹ The majority of published research had focused on the effects that gene expressions, growth factors and cell communications play in the embryonic differentiation. Recently, there have been discussions that the nanoscale features of material surfaces can be used to control cellular behavior^{2, 3} and that elasticity of the extracellular matrix can regulate mesenchymal stem cell differentiation.^{4,5} More detailed morphological *in situ* characterization of cell supporting scaffolds before and during cell culture as well as correlating the role of scaffolds' architecture to stem cells' behaviors are necessary for the development of successful applications.

Collagen hydrogels play an important role as scaffolds in tissue engineering and regenerative medicine. The 3D architecture of scaffolds composed of collagen type I, includes micron-sized fibers that constitute the solid phase and effective pores, which are interconnected channels containing a fluid phase.⁶ Optical properties and the overall architecture of collagen hydrogels is inevitably altered by changing physicochemical self-assembly conditions⁷ including temperature⁸ and collagen biopolymer solid content⁸ as well as by adding cross-linkers. The above manipulations can further simultaneously change ligand type and/or ligand density sensed by the cells, mechanical strength of scaffolds and structures within. Earlier research emphasized mechanical properties of scaffolds in driving differences in cellular behaviors.⁹ More recent studies uncovered importance of microstructures defining these mechanical properties.^{10, 11} At present, the microstructure, which is one of the elements needed to rationally engineer functional tissues, organs and model systems is also one of the least explored.

Multiphoton Microscopy (MPM) is a nondestructive optical method that can be used to image directly and in real time the microstructure within collagen systems *in situ* in three dimensions with high resolution and contrast. It employs femtosecond pulses of near-infrared (NIR) laser light, which reduces scattering and affords deeper sample penetration compared to confocal and traditional microscopy-based techniques. The intrinsic second harmonic generation (SHG) and two-photon fluorescence (TPF) contrasts used in MPM emerged as valuable label-free spectroscopic probes that can provide complementary information regarding microstructure in thick tissue,¹²⁻¹⁷ biomaterial^{7, 8, 18-24} and wound examinations.²⁵⁻²⁸ SHG contrast is used to directly detect aggregated collagen structures (fibers) within scaffolds. It resists photobleaching and is generated when NIR photons that interact with fibrillar collagen are combined to produce new photons at twice the energy. TPF detects fluorophores initially present or in this work induced as a result of modifying collagen with a chemical cross-linker genipin.

We aimed to envision possible scenarios of how stem cells could be found to interact with collagen scaffolds when used in tissue engineering/regenerative medicine applications. To that extent we prepared nine different stem-cell models (**Table 1**) that employ 3D collagen hydrogels and mammalian embryonic G-Olig2 stem cells (green fluorescence protein (GFP) inserted into the locus of Olig2²⁹). The parameters varied in preparation of 3D collagen hydrogels were: (1) collagen biopolymer solid content; (2)

self-assembly temperature; (3) cross-linking type and degree varied through stabilization with a zero-crosslinker carbodiimide (EDC) and EDC/N-Hydroxysuccinimide (NHS) or a non-zero crosslinker genipin and (4) the environment type varied through embedding or surface depositing stem cells within/on the scaffolds.

We chose 2 g/l and 4 g/l collagen concentrations because they covered the range commonly used in tissue engineering. These concentrations produce significantly different physical microenvironments resembling provisional or immature extracellular matrix that occurs during development. The 1.8 g/l was the lowest concentration at which using the assembly conditions in this work, we could still form hydrogels,⁸ compelling us to use concentrations above this critical value. The cellular behavior and collagen fiber structure could be clearly visualized in the low concentration 2 g/l gels. The 4 g/l gels could be readily made from the stock solution concentrations of eight to nine g/l we carry in the laboratory and served as a 'high' endpoint in establishing materials.

Our main goal was to provide further characterization of the synthesized materials and to better understand and quantify behavior of the cultured embryonic stem cells on/within them *in situ* by employing MPM imaging method. The properties characterized were: (1) collagen fiber and effective pore structure within hydrogels prior to and during cell culture, (2) degradation pattern and degradation kinetics of hydrogels with collagenase, (3) the aspect ratios of cellular components during cell culture, (4) optical properties of hydrogels stabilized with genipin, (5) storage and loss moduli of all materials. The prepared hydrogels are biodegradable, the chosen chemical cross-linkers are nontoxic and the *in situ* MPM method employed to characterize the models is nondestructive to biological samples. All seem highly valuable for biological applications. The data and methods developed provide an outline to monitor non-

	Environment Type	Cross-linker	Collagen Hydrogel Preparation Conditions	
			Temperature (°C)	Collagen Solid Content (g/l)
1	Encapsulated	None	37	2
2	Encapsulated	None	37	4
3	Topographic	None	37	2
4	Topographic	None	37	4
5	Topographic	None	27	2
6	Topographic	None	27	4
7	Topographic	EDC	37	2
8	Topographic	EDC/NHS	37	2
9	Topographic	Genipin	37	2

Table 1. Summary of the embryonic stem-cell models that employed 3D collagen hydrogels.

1
2
3 destructively *in situ* behaviors of cells during cell culture on and within thick,
4 scattering collagen-based substrates in regenerative medicine and tissue engineering
5 applications. Furthermore, it demonstrates the utility of multiphoton microscopy in the
6 stem cell and other biology-related research, which is novel and timely.
7
8

9 **Materials and Methods**

10 **1. Advanced characterization of synthesized collagen hydrogels**

11 **Crosslinking Degree Assay**

12 We used the ninhydrin colorimetric method to determine the extent of modification of
13 amino groups with cross-linking reagents within collagen hydrogels. The percentage of
14 the remaining free amines after cross-linking was calculated to establish the relative
15 cross-linking degree. 100 μ l of sample mix of the following final composition were
16 added to a well of 96 well plate: 30 mM phosphate buffer, [NaCl] = 0.3 M, [collagen] = 2
17 g/l, pH 7.4 and incubated under 37 $^{\circ}$ C for 24 hours. The 100 μ l same-day-prepared 1 mM
18 genipin or 0.1 M EDC or 0.1 M EDC/0.025M NHS solutions (in 30 mM phosphate
19 buffer, [NaCl] = 0.3 M, pH=7.4) were added on top of collagen hydrogels and incubated
20 for another 24 hours under 37 $^{\circ}$ C. The control samples were incubated in 30 mM
21 phosphate buffer, [NaCl] = 0.3 M, pH = 7.4 for the same duration of time. The cross-
22 linking reagents were removed by adding double deionized H₂O (ddH₂O) and incubating
23 for at least 30 min. This washing procedure was repeated at least three times.
24 Subsequently, 10 μ l of 2 g/l collagenase were added to samples, adjusted to the volume
25 of 650 μ l with ddH₂O and incubated for 72 hours at 37 $^{\circ}$ C. 350 μ l of 2 % ninhydrin stock
26 (in ethanol) were added to each sample and boiled for 2 min. UV-Vis-NIR
27 spectrophotometer (Varian, Carry 500) was used to detect the absorbance of samples in
28 the range of 300 – 900 nm. Different concentrations of glycine solution, 10 μ l 2 g/l
29 collagenase solution and 350 μ l 2 % ninhydrin stock solution (in ethanol) were used to
30 construct the calibration curve and repeated at least three times. Cross-linking degree was
31 then calculated as: crosslinking degree = $(1 - (\text{cross-linked Absorbance}_{570}/\text{non-cross-}$
32 $\text{linked Absorbance}_{570})) * 100\%$. All samples were prepared in triplicates. For the cross-
33 linked hydrogels the cross-linking degree was: a) genipin-cross-linked hydrogel: 87%; b)
34 EDC/NHS-cross-linked hydrogel: 60%; c) EDC-cross-linked-hydrogel: 12%. The
35 chemical modifications with the above reagents result in the formation of the covalent
36 bonds between collagen molecules and are stable overtime (unpublished data).
37
38
39
40
41
42
43
44
45
46

47 **Enzymatic Degradation Assay**

48 The samples were prepared between No. 1 coverslip, separated with a 2.3 mm
49 thick silicone gasket having an 18 mm round opening. All the preparations were done
50 under sterile conditions on ice. 600 μ l collagen hydrogel mix of the following final
51 composition was used per sample: 30 mM phosphate buffer, [NaCl] = 0.3 M, [collagen] =
52 2 g/l, pH 7.4. To gel the samples we incubated them for 2 hours at the specified
53 temperature. For the cross-linked hydrogels, the 50 μ l of cross-linker solutions prepared
54 at 10 \times concentration in 30 mM phosphate buffer, [NaCl] = 0.3 M, pH = 7.4 were added
55 on top of collagen hydrogels. The hydrogels were subsequently incubated with cross-
56 linkers for 24 hours at 37 $^{\circ}$ C. To remove the cross-linkers, we incubated the hydrogels
57
58
59
60

1
2
3 with 30 mM phosphate buffer, pH = 7.4, [NaCl] = 0.3 M for 20 minutes at room
4 temperature. The cross-linker removal procedure was repeated at least three times. To
5 digest the materials, we added 50 μ l of collagenase (C0130, Sigma) activated with buffer
6 as specified in the supplied instructions.
7
8

9 **Rheology Measurements**

10 Rheological measurements were carried out with a computer interfaced Haake
11 RheoStress 1 temperature controlled parallel plate rheometer. The sensor diameter was 35
12 mm and the measurements were carried out at the specified temperatures. Oscillation
13 amplitude sweeps were performed in the controlled stress (CS) mode to establish the
14 viscoelastic linear regions for the non-cross linked hydrogels. The frequencies used were
15 0.5 Hz, 0.7 Hz and 1 Hz. The gap was re-calibrated prior to daily measurements. The
16 samples for synthesis of collagen hydrogels were prepared as described previously.⁷
17 Briefly, 550 μ l of self-assembly mix were loaded on the bottom plate of the rheometer
18 preheated to the desired temperature. The gap was adjusted by lowering the top plate to
19 create 0.2 mm distance between the two plates. The hydrogels were allowed to
20 polymerize (20 min at 37 °C or 50 min at 27 °C) and the rheology data was collected.
21 Oscillation frequency sweep (0.1 – 50 Hz) controlled deformation (CD) mode rheology
22 data was obtained with the strain rate of 0.05.
23
24

25 For measurements on the cross-linked hydrogels, the gap was 2 mm. 2 g/l 24-hr
26 37 °C pre-polymerized collagen hydrogels were separately incubated with cross-linkers
27 (1 mM genipin, 0.1 M EDC or 0.1 M EDC+0.025 M NHS) for 24 hours at 37 °C. Upon
28 transferring them to the bottom plate of the rheometer, we carried out oscillation
29 frequency sweep (0.1 – 50 Hz) rheology measurements (strain rate 0.05) in a controlled
30 deformation (CD) mode.
31
32
33

34 **Spectral measurements**

35 All UV-Vis spectra were obtained with UV-Vis-NIR spectrophotometer (Varian,
36 Carry 500). The multi-photon spectra were acquired with a 10 \times , 2.6 mm working
37 distance, N-Acroplan, water immersion objective (Zeiss, 420947-9900-000, N.A. 0.3) in
38 the epi-collected configuration.¹⁸ The spectra were filtered from the laser excitation with
39 a long pass 705 nm single-edge dichroic beamsplitter (Semrock, FF705-Di01-34 \times 46) and
40 additionally filtered through a 720 nm short pass filter (Semrock, FF01-720/SP-25)
41 introduced at the original exit port of the modified Zeiss Axioexaminer.Z1. Spectra were
42 obtained with Acton SP2300 spectrograph equipped with a 68 mm \times 68 mm, 300
43 grooves/mm ruled grating blazed at 500 nm and a Pixis1024B CCD camera (Princeton
44 Instruments, Trenton, New Jersey). The spectrograph and camera settings were PC-
45 controlled through WinSpec/32 v.2.5K software. The CCD temperature was maintained
46 at -75 °C in all the experiments to ensure low dark noise. The entrance slit of the
47 spectrograph was set to a width of 1 mm. A typical spectral acquisition time was 16 s.
48 The multiphoton spectra were corrected for dark noise background and obtained under
49 equivalent power and other settings for different samples and wavelengths.
50
51
52
53

54 **Multiphoton microscopy (MPM) imaging**

55 The inverted multiphoton laser-scanning microscope used in this work was the
56 Zeiss LSM 510 NLO Meta microscopy system. It is based on an Axiovert 200M inverted
57
58
59
60

1
2
3
4
5
6
7
8
9
10
11
12
13
14
15
16
17
18
19
20
21
22
23
24
25
26
27
28
29
30
31
32
33
34
35
36
37
38
39
40
41
42
43
44
45
46
47
48
49
50
51
52
53
54
55
56
57
58
59
60

microscope equipped with standard illumination systems for transmitted light and epifluorescence detection. It was also equipped with an NLO interface for a femtosecond titanium:sapphire laser excitation source (Chameleon-Ultra, Coherent, Incorporated, Santa Clara, CA) for multiphoton excitation. The Chameleon laser provided femtosecond pulses at a repetition rate of 76 MHz, with the center frequency tunable from 690 to 1040 nm. A long working distance objective (Zeiss, 40× water, N.A. 0.8) was used to acquire images shown in this work. The signals from the samples were epicollected and discriminated by long pass 650 nm dichroic beamsplitter. The SHG images were collected with the 390-405 nm band-pass filter ($\lambda_{\text{ex}} = 800$ nm). The two-photon fluorescence (TPF) images were collected with the 390 – 465 nm + 530–590 nm band-pass filters and $\lambda_{\text{ex}} = 770$ nm. Unless noted, the images presented in this work are 12 bit, 512×512 pixels representing $225 \mu\text{m} \times 225 \mu\text{m}$ field of view. The multiphoton images were obtained from at least four gel replicates. Typically, two independent samples were imaged per day. Imaging was repeated at least one more time on another completely independent set consisting of two samples. Many fields of view (10 and more) were acquired per each sample and the representative images are shown in the figures.

To confirm validity and reproducibility of our imaging observations, randomly selected samples were additionally re-imaged on the upright Thorlabs Laser Scanning Multiphoton Microscope.⁷ This upright Nikon microscope was used to obtain images used to follow degradation of collagen hydrogels with collagenase and to construct degradation kinetics data plots. It is equipped with a femtosecond titanium:sapphire laser excitation source (Mai-Tai HP, Spectra Physics, Santa Clara, CA) that provided femtosecond pulses at a repetition rate of 76 MHz, with the center frequency tunable from 690 to 1040 nm. Long working distance (2 mm to 2.6 mm imaging range) aberration corrected UV-VIS/near IR imaging/excitation water immersion objectives (Zeiss, 63× water, N.A. 1.0; Zeiss 10× water, N.A. 0.4 and Olympus 20× water, N.A. 1.0) were used as needed. Spectral filtering with dichroics and bandpass filters was used to separate second harmonic generation (SHG) and two-photon excited fluorescence (TPF) signals as indicated in the text. Each image acquired was 2048×2048 pixels, which corresponds to $700 \mu\text{m} \times 700 \mu\text{m}$ field of view for Olympus 20× water objective (Olympus, XLUMPLFLN, N.A. 1.0, 2.0 mm working distance). For the degradation experiments, the samples are placed onto the in-house build temperature controlled stage adaptor made from anodized aluminum kept at 32 °C. We imaged the top 500 μm within the materials, throughout the duration of the degradation experiments. We imaged all the necessary controls for the same time durations and under the same conditions as the samples that were degraded with collagenase. To ensure reproducibility, all the experiments were repeated on different days and at least two times. The in-house written Matlab code was used to evaluate SHG and TPF signals averaged intensities by calculating the average pixel values in the acquired images.

The SHG or TPF signal averaged intensities were plotted as a function of depth to obtain attenuation curves.²³ Briefly, at different laser focus depths, there are different values of SHG and TPF signals. As the laser focus is moved deeper into the samples by adjusting the vertical position of the focusing objective, the SHG and TPF signal intensities first build up, reach maxima and then decay due to both attenuation of excitation and decrease in the collection efficiency of the scattered signals. In all the degrading samples, we observed that the degradation with collagenase would take place

1
2
3 starting at the top of the materials where we applied it. Therefore, we found that SHG or
4 TPF signal attenuation curves were moving as the signals were progressively attenuated
5 due to materials' degradation. The SHG or TPF signal attenuation curves remained
6 stationary for the controls (no collagenase was applied) imaged for the same time
7 durations and under the same conditions. To obtain the kinetic traces, we selected
8 signal intensity values at the same imaging depths, which coincided with a top of the
9 attenuation curve obtained at the zero time point. Plan-Apochromat water immersion
10 63 \times , 2.1 mm working distance objective (Zeiss, 421480-9900-000, N.A. 1.0) was
11 employed to obtain images used to evaluate porosity of the degrading hydrogels. We first
12 obtained SHG or TPF signal attenuation curves. We would subsequently measure
13 porosity at a section around the area of possible maximum in SHG or TPF signal
14 attenuation curves collected at zero degradation time. We followed the changes in the
15 effective pore structure size at the selected depth for the duration of the degradation
16 experiment. These experiments were repeated at least three times and at least fifty
17 effective pore structure sizes were measured.

18
19 To obtain the % of materials degraded after 24 hours of digestion, we imaged the
20 height of materials from the side opposite to where collagenase was added and divided by
21 an original 2 mm height of the materials.

22
23 The network structural parameters such as collagen fibers length, width and pore
24 dimensions were quantified with either LSM software or ImageJ
25 (<http://imagej.nih.gov/ij/>) and the error bars are the standard deviations from the mean
26 values. Between twenty and fifty independent measurements of each parameter were
27 performed for each experimental system. For the cell-containing samples where the
28 collagen fiber distribution was very heterogeneous, the measurements were grouped into
29 separate categories (long and short fibers). We used a straight forward method of
30 measuring the resulting fibers' lengths by tracing along the fibers, reproducibly attaining
31 the measured numbers.

32
33 To determine how spherical (round) the cellular components are in our models we
34 used images to determine their aspect ratios. The aspect ratio was estimated as a percent
35 of sphericity by calculating width to length ratio. Between fifteen and twenty independent
36 measurements were performed to establish estimates. The aspect ratio of 100% indicates
37 a perfectly round cell/cell cluster while small numbers indicate extended, slender objects.
38 The errors were calculated as the standard deviations of the mean.

39 40 41 42 43 44 **2. Collagen hydrogel three-dimensional cellular models**

45 46 **Murine embryonic stem cell culture**

47 Cells of the embryonic stem cell line G-Olig2 (ATCC, SCRC-1037) were cultured
48 on mouse embryonic fibroblasts (ATCC, CCL163) in Advanced DMEM (Dulbecco's
49 Modified Eagle Medium, 12491) with 0.1 mM β -mercaptoethanol (Sigma) and Leukemia
50 Inhibitory Factor (LIF) at a concentration of 1000 U/ml. The cell culture medium was
51 changed daily.

52 53 **Three-dimensional encapsulated cellular model**

54 The final collagen concentrations used in this work were 2.0 g/l and 4.0 g/l. An
55 ice-cold collagen mix was prepared consisting of 6.5 parts of collagen type I (BD
56 Biosciences, 354249), 1 part of reconstitution buffer (10 \times) and 2 parts of DMEM growth
57
58
59
60

1
2
3 medium (Gibco Cat. No. 12800-058, 5×). For the 6.5 parts of collagen solution, 3.0 g/l
4 was used for the final concentration of 2.0 g/l and 6.2 g/l was used for the final
5 concentration of 4.0 g/l. The 3.0 g/l and 6.2 g/l collagen solution was corrected from the
6 8.58 g/l collagen stock.
7

8 The 10× reconstitution buffer was prepared by combining 2.2 g of NaHCO₃
9 (tissue culture grade) and 4.77 g HEPES (tissue culture grade, Gibco Cat. No 845-1344)
10 in a 100 mL medium bottle, adding 75 mL of 0.05 N NaOH (5 mL of 1 N NaOH [Fisher,
11 SS266-1] added to a 95 mL of doubly distilled, deionized water) to the sodium
12 bicarbonate and HEPES powder, mixing well to dissolve and bringing solution to the
13 final volume of 100 mL with 0.05 N NaOH. The buffer was sterilized with 0.22 μm filter
14 into a sterile medium bottle and stored at 4 °C. After three components were mixed and
15 pH was adjusted to neutral, cells in 0.5 parts of 1× PBS buffer were added to the mixture.
16 The mixture was added into each well of 8-well chambered coverglass (MP Biomedicals)
17 and incubated at 37 °C until the gels were formed. The number of cells in each gel was
18 3×10⁴. All procedures were performed under the BSL-II cell culture hood and employing
19 sterile techniques. The stock solution of retinoic acid at concentration of 2 × 10⁻⁵ M was
20 prepared by dissolving retinoic acid (Sigma, R2625) in DMSO (Sigma, D2650). The
21 stock solution was filtered with 0.2 μm nylon filter (Corning, 431224) and stored at -80
22 °C. The stock solution of retinoic acid was diluted with Advanced DMEM to bring the
23 concentration to 2 × 10⁻⁶ M and added to each gel starting at day 0. The retinoic acid was
24 refreshed daily. This concentration of retinoic acid and frequency of treatments were
25 shown to induce embryonic stem cell differentiation to neuronal lineage cells.³⁰⁻³³
26
27
28
29
30

31 **Three-dimensional topographic cellular model**

32 3D collagen hydrogels were prepared as described previously.¹⁸ The stock
33 concentration of soluble rat-tail type I collagen was 8.58 mg/mL (BD Biosciences). The
34 final pH was 7.4 ± 0.1 and the hydrogels were polymerized either at 27 °C or 37 °C. The
35 materials were prepared in the 8-well chambered coverglass (MP Biomedicals). The final
36 collagen concentration of the materials (solid content) was 2.0 g/l or 4 g/l as noted. 1 mM
37 genipin was prepared by dissolving genipin (Sigma) in PBS buffer and adjusted to pH 7.4
38 with 1 N NaOH. The genipin solution was sterilized with a 0.22 μm filter (Millipore,
39 Millex GV Filter, Cat # SLGV003RS) and kept at 4 °C. Fresh 1 mM genipin solution was
40 added to each gel-containing well. The self-assembled 2 g/l collagen hydrogels were
41 incubated at 37 °C in presence of 1 mM fresh genipin solution for 24 hrs. After 1 day of
42 incubation, the genipin solution was removed, 1× PBS buffer (Invitrogen, Dulbecco's
43 Phosphate-Buffered Saline, 14190) was added, incubated with materials for 20 min at
44 room temperature and subsequently removed. This procedure was repeated at least 3
45 times to remove the cross-linking reagent. The incubation with 0.1 M EDC and 0.1 M
46 EDC/0.025M NHS solutions (Sigma) was at 37°C for 24 hr and the reagents were
47 removed in a similar manner. Prior to cell culture, the cross-linked gels were equilibrated
48 with Advanced DMEM for 24 hrs at 37 °C. For seeding on collagen gels, 3×10⁴ cells
49 were added to each gel and incubated at 37 °C for 3 hrs. When after 3 hrs cells attached
50 to gels, we treated them with retinoic acid in a manner identical to encapsulated cellular
51 models.
52
53
54
55
56
57
58
59
60

Results

1. Advanced characterization of synthesized collagen hydrogels

1.1 Optical properties and microstructure of synthesized collagen hydrogels

When we treat the opaque collagen hydrogels with clear solutions of fresh 1 mM genipin at pH 7.4 and room temperature, a noticeable blue-grey color³⁴ corresponding to ~590 nm absorbance (**Figure 1B, left**) and two-photon fluorescence (TPF) (**Figure 1B, right**) develop within 24 hours. The TPF spectra exhibits two peaks centered at ~490 nm and at ~615 nm. The ratio of the intensity of 615 nm emission band to the intensity of 490 nm emission band is five and does not change significantly at longer modification times (72

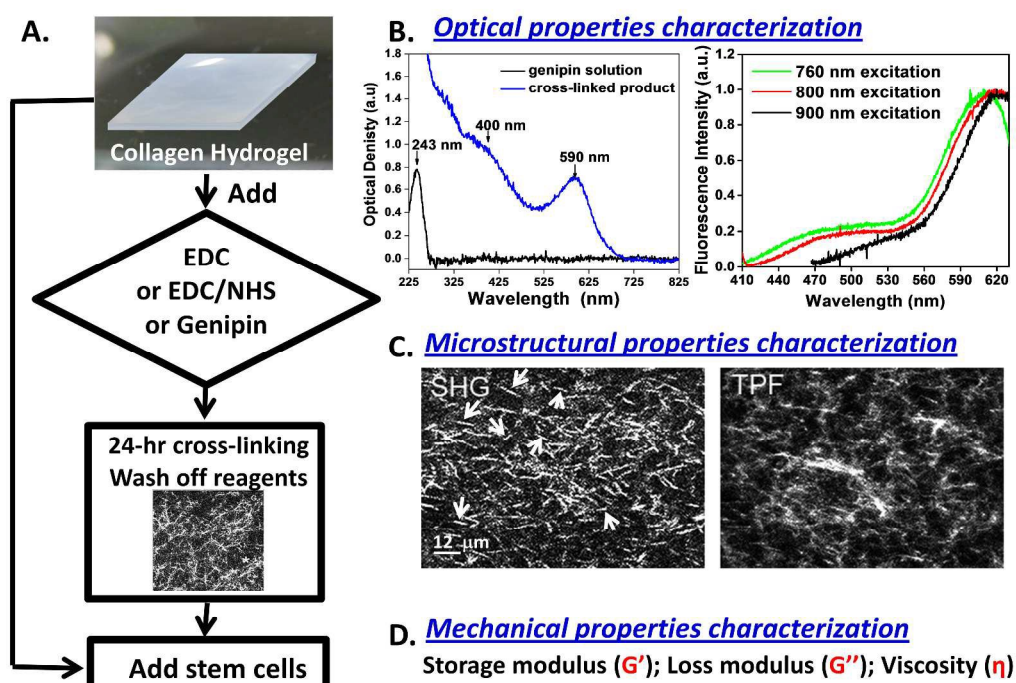


Figure 1. The experimental schematic. (A) Overview of an experimental strategy; (B) Typical one photon absorbance spectrum (left). The one photon absorbance spectrum of fresh genipin solution used to modify materials is shown for comparison. Typical two-photon fluorescence (TPF) spectra (right) of genipin modified collagen hydrogels; (C) Second harmonic generation (SHG) images ($\lambda_{\text{ex}}/\lambda_{\text{em}} = 810 \text{ nm}/400\text{--}410 \text{ nm}$, white arrows point to the white fibers; effective pores are the black spaces between the white fibers) and two-photon fluorescence (TPF) images ($\lambda_{\text{ex}}/\lambda_{\text{em}} = 810 \text{ nm}/470\text{--}550 \text{ nm} + 570\text{--}610 \text{ nm}$) of a genipin-modified hydrogel; (D) The output mechanical properties such as storage modulus G' , loss modulus G'' and viscosity η of the prepared materials were characterized as well.

hrs). There is a very slight bathochromic (red) shift of fluorescence when the excitation wavelength is varied between 760 and 900 nm. Fluorescence from non-crosslinked gels is negligible compared to genipin cross-linked gels when excited with wavelengths we

used. For example, in the two photon spectrum of a non-cross-linked gel, an excitation at 800 nm, leads only to a second harmonic generation (SHG) signal at 400 nm that can be readily seen (Figure S1).

Figure 2 shows that the genipin-modified hydrogels generate approximately five times less SHG signal compared to non-modified controls (24 hours of modification at 37 °C). On the other hand, as determined from the average TPF image intensities, TPF collected in 470 – 550 nm spectral region (TPF #1) increases two fold and TPF collected in 570 – 610 nm spectral region (TPF #2) increases nine fold compared to non-modified control hydrogels.

In **Table 2**, we report sizes of collagen fibers and effective pores within hydrogels quantified from SHG and TPF images of synthesized hydrogels prior to stem cell culture. The 27 °C self-assembly temperature produces longer and thicker fibers separated by larger effective pores compared to those formed at 37 °C. As determined from SHG images, upon treating collagen hydrogels with zero-length cross-linker EDC,¹⁸ with or without addition of NHS, the microstructure within gels remains the same (the molecular

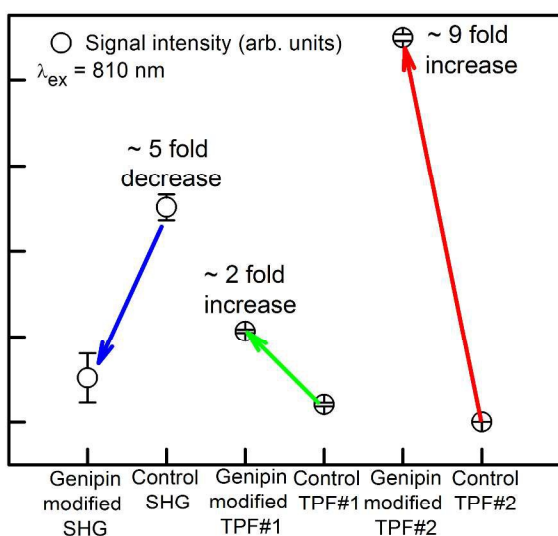


Figure 2. Quantifying genipin cross-linking reaction with collagen within hydrogels. The hydrogels were prepared at 0.3 M sodium chloride, pH 7.4, 30 mM phosphate, 37 °C polymerization temperature, 2 g/l collagen solid content. After 24-hour incubation, samples were modified for another 24 hours by 1 mM genipin solution adjusted to pH 7.4. The optical filter used to acquire SHG signals was 405±5 nm. The spectral range of acquired TPF#1 was 470 – 550 nm. The spectral range of acquired TPF#2 was 570 – 610 nm.

Depending on the experiment, these types of kinetics profiles were obtained by following SHG or TPF signals as a function of time. The typical data for 2 g/l 37 °C materials shows microstructure of a collagen hydrogel immediately after collagenase solution was

changes, however, are detectable with Raman microspectroscopy³⁵). Upon cross-linking with a genipin reagent,²¹ ~5 μ m long SHG-generating fibers present within hydrogels prior to cross-linking reaction ‘wash out’ leading to less strong second harmonic generation (SHG) contrast. Newly induced TPF-generating fibers are less well structured and are significantly longer (~19 μ m, Table 2) than initially present SHG-generating fibers.

1.2. Enzymatic degradation assay of synthesized collagen hydrogels

To evaluate the enzymatic degradation of our synthesized materials, we typically applied a solution of collagenase to collagen hydrogels and with multiphoton optical imaging method: a) for ~24 hours continuously imaged *in situ* the degradation of collagen gels; b) quantified percent of materials left after 24 hours of degradation. **Figure 3** shows a typical *in situ* degradation kinetics profile of collagen hydrogels.

topically added (**Figure 3A**) and 25 min later (**Figure 3B**). For all non-cross-linked collagen gels, regardless of the hydrogel preparation condition, the half-time for degradation was approximately fifteen minutes. Tables in **Figure 3** summarize the observed increase in collagen hydrogels' porosity detected in real time *in situ* during degradation reactions.

All non-cross-linked collagen hydrogels completely degraded after 24 hours while cross-linked hydrogels showed enhanced stability. For the genipin-cross-linked materials, after 20 hrs of degradation, hardly any material was removed by

Collagen Hydrogel Preparation Condition	Collagen Hydrogel Microstructural Parameters
	Fiber Length Fiber Width Effective Pore Diameter; all in (μm) \pm St. Dev.
37 °C, 2 g/l	4.8 \pm 1.1
	0.95 \pm 0.2
	5.2 \pm 1
37 °C, 4 g/l	4.6 \pm 0.8
	1.0 \pm 0.1
	3.0 \pm 0.5
27 °C, 2 g/l	43 \pm 8.4
	7.1 \pm 1.4
	50.2 \pm 10.8
27 °C, 4 g/l	51.5 \pm 7.2
	6.61 \pm 1.7
	40 \pm 11.5
37 °C, 2 g/l, EDC-crosslinked	6.13 \pm 1
	1 \pm 0.12
	5.6 \pm 1.4
37 °C, 2 g/l, EDC/NHS-crosslinked	6.18 \pm 0.9
	1.0 \pm 0.1
	8.19 \pm 1.2
37 °C, 2 g/l Genipin-crosslinked – SHG contrast	2.9 \pm 0.6
	0.7 \pm 0.2
	5.1 \pm 1.1
37 °C, 2 g/l Genipin-crosslinked – TPF contrast	19.3 \pm 3.9
	3.4 \pm 1.4
	17.4 \pm 4.5

Table 2. Summary of the collagen hydrogel microstructural parameters and corresponding standard deviations from the mean. The hydrogels were prepared at 0.3 M sodium chloride, pH 7.4, 30 mM phosphate, 37 °C or 27 °C self-assembly temperatures and collagen solid content of 2 g/l or 4 g/l. Additionally, some hydrogels were separately cross-linked with carbodiimide (EDC), carbodiimide (EDC)/N-Hydroxysuccinimide (NHS) or genipin.

collagenase. Thus for the conditions we sampled, no time constants could be determined. The situation was similar for the EDC+NHS crosslinked collagen hydrogels and EDC-crosslinked collagen hydrogels at the spots where we collected kinetics data.

The percent of each material left after 24 hours of degradation with collagenase is shown in **Figure S2**. Genipin stabilized hydrogels are nearly 94% intact after 24 hours of degradation. EDC cross-linked hydrogels show great spatial variability of degradation and there is ~30% to 80% of material that remains intact depending on the location sampled. EDC/NHS cross-linked hydrogels exhibit medium degradability with 75% of the material remaining intact at 24 hours of degradation with collagenase.

1.3. Rheology analysis of synthesized hydrogels

The linear regime in which collagen gels exhibit equilibrium storage modulus is 8% for 27 °C self-assembled gels and 40% for 37 °C self-assembled gels (data not shown) with

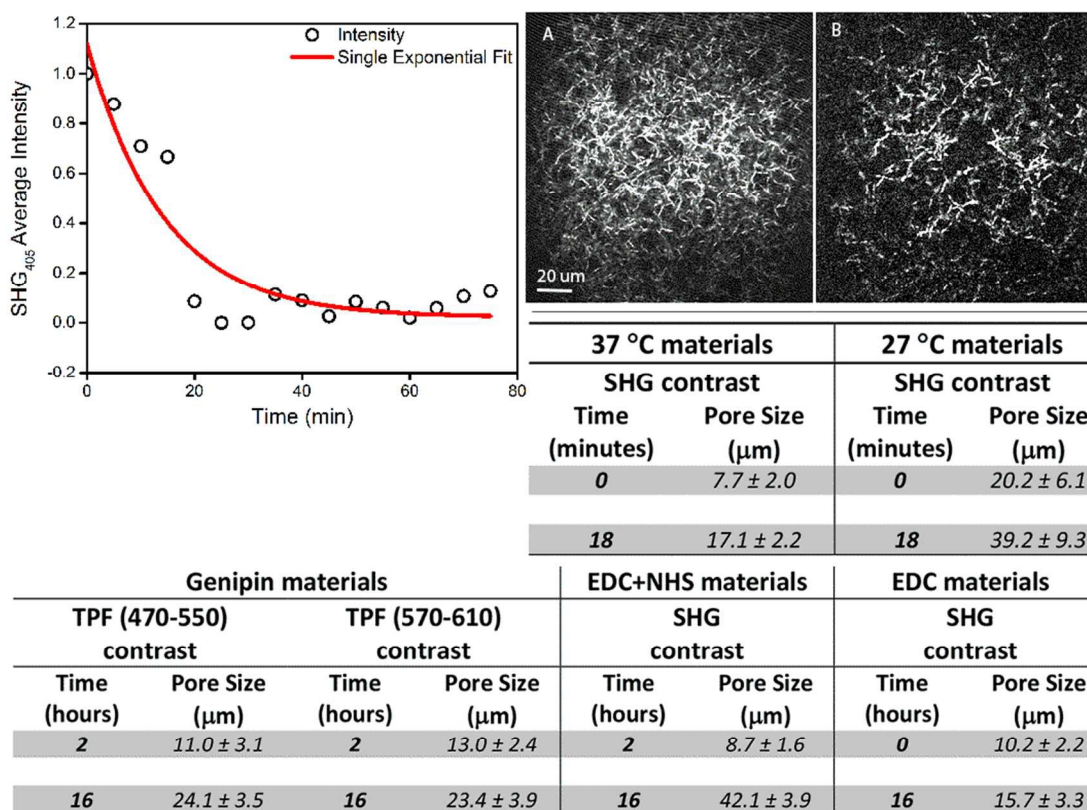


Figure 3. The effect of collagen hydrogels' digestion by a topically applied collagenase solution. Typical *in situ* degradation kinetics plot for 2 g/l 37 °C polymerized non-cross-linked hydrogel (Left). Second Harmonic Generation (SHG) images collected with 20× Olympus objective show microstructure of a collagen hydrogel immediately after collagenase solution was added (A) and 25 min later (B). Tables (Bottom) summarize the porosity of collagen hydrogels detected in real time during degradation with collagenase.

the latter exhibiting a strain-stiffening response.³⁶ For unmodified hydrogels, the viscosity, storage modulus G' and loss modulus G'' all increased with increasing collagen solid content from 2 g/l to 4 g/l for hydrogels prepared at both 37 °C and 27 °C incubation temperatures (**Figure 4**). The data shown is for 0.1 Hz frequency.

Supplementary information **Figure S3** shows the dynamic mechanical properties for 2 g/l and 4 g/l collagen gels prepared at 27 °C and 37 °C. For all the materials, the average storage modulus G' is always higher than the loss modulus indicating that the hydrogels have polymerized into solid materials prior to measurements. The measured dynamic mechanical properties (viscosity, G' , G'') reach higher values for hydrogels prepared at 27 °C compared to the materials prepared at 37 °C. Nevertheless, the variability in the measured mechanical parameters for 27 °C self-assembled samples is also greater. Therefore, no significant difference in the mechanical properties for hydrogels self-assembled at 27 °C versus 37 °C could be reliably measured for either 2 g/l or 4 g/l gels. The values of loss tangent ($\tan \delta = G''/G'$) are 0.24 to 0.35 with the highest value of 0.35 for 2 g/l 27 °C hydrogels.

As seen in **Figure 4**, the storage modulus (G') is 40%, 60% and 90% higher in EDC, EDC/NHS and genipin cross-linked materials respectively compared to non-cross-linked controls. The loss modulus (G'') is 40% and 70% higher in EDC/NHS and genipin cross-linked materials compared to non-cross-linked controls. The variability in the measured G'' values for EDC-cross linked materials is high and therefore, no significant difference in these values compared to non-cross-linked controls is reliably detected. The value of loss tangent ($\tan \delta = G''/G'$) is the lowest for genipin-stabilized hydrogels. The loss tangent calculated (0.17) is lower by nearly 45% compared to non-cross-linked controls. This indicated that a G'' viscose component decreased concomitantly with an increase in the G' elastic modulus.

2. Characterization of the collagen hydrogel three-dimensional cellular models with in-situ TPF and SHG contrasts.

2.1. 37 °C 3D encapsulated models at 2 g/l or 4 g/l collagen solid content: The encapsulation of stem cells in collagen hydrogels can potentially be an effective method to deliver them to injured areas. We encapsulated stem cells directly within hydrogels prepared either at 2 g/l or 4 g/l collagen solid content and 37 °C self-assembly temperature. To identify stem cells in the models, we acquired true focus (**Figure 5A**) and endogenous two-photon fluorescence (TPF) (**Figure 5B**) images. The TPF images of cells are obtained from the same optical section as second harmonic generation (SHG) images of collagen microstructure within hydrogels (**Figure 5C**) while true focus images carry information from optical planes through the entire thickness of hydrogels. All images in **Figure 5** were obtained on day six of cell culture and show that the extension rate of stem cells encapsulated in 4 g/l collagen hydrogels is slower compared to 2 g/l materials. For cells embedded in 4 g/l collagen hydrogels, the aspect ratio is $83\% \pm 6\%$ indicating almost perfectly round objects. The aspect ratio is $17 \pm 5\%$ for cells embedded in 2 g/l collagen hydrogels signifying that cells elongated.

Cultured stem cells do not modify the microstructure of 4 g/l collagen hydrogels while the highly processed hydrogel architecture is seen in the SHG images of 2 g/l collagen models (**Figure 5F**). We could resolve invaginations formed at the points where there are contacts of cells and collagen. Both short and long collagen fibers were detected within these materials. The short fibers are $2.4 \pm 0.6 \mu\text{m}$ in length, which is similar to collagen fibers within hydrogels prior to cell culture. The newly induced long fibers are $15.4 \pm 2.8 \mu\text{m}$ in length (**Figure 5**, table beneath). In 4 g/l 37 °C models, the fiber length remains similar to that found in collagen hydrogels prior to cell culture. The fiber widths remain similar to controls ($\sim 1 \mu\text{m}$) in both 2 g/l and 4 g/l 37 °C models. In a 2 g/l 37 °C model the effective pore size (**Figure 5**, table beneath) is somewhat smaller ($\sim 2 \mu\text{m}$) compared

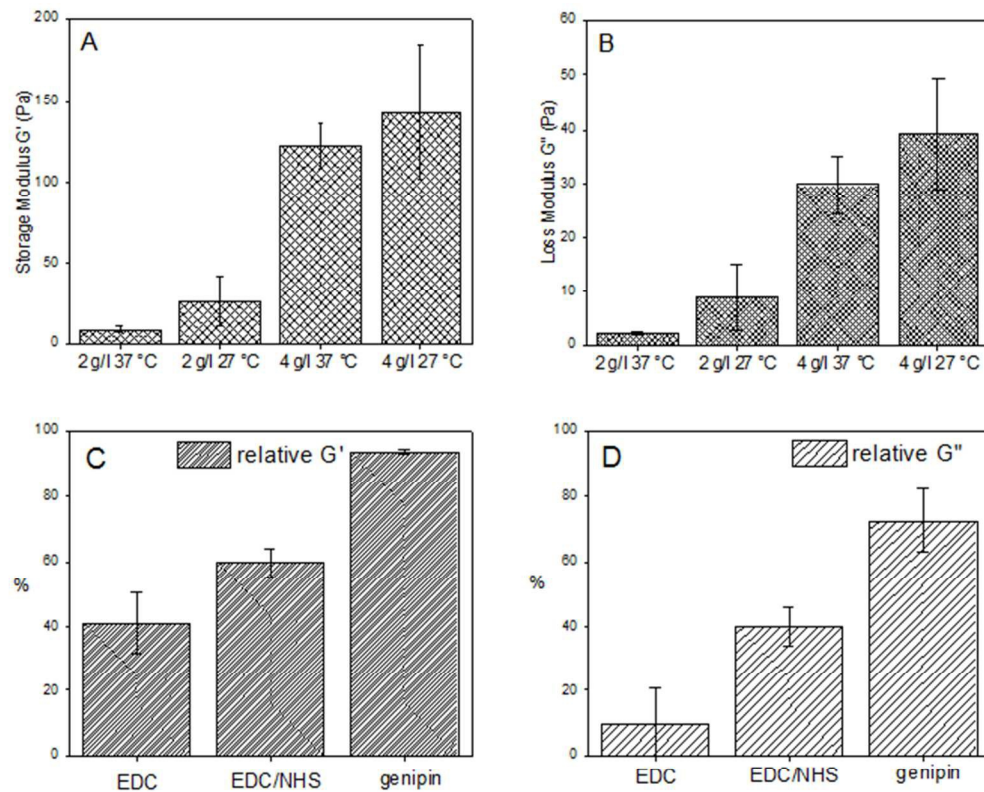


Figure 4. Storage moduli G' for collagen hydrogels prepared at different collagen solid content and self-assembly temperatures (A); Loss moduli G'' for collagen hydrogels prepared at different collagen solid content and polymerization temperatures (B); Relative storage moduli G' for collagen hydrogels cross-linked with EDC, EDC/NHS and genipin reagents (C); Relative loss moduli G'' for collagen hydrogels cross-linked with EDC, EDC/NHS and genipin reagents (D). For non-cross-linked gels, the data plotted is for 0.1 Hz frequency and error bars reflect the standard deviations from the mean measured values. For cross-linked gels, the data plotted is an average for 0.1 – 1 Hz frequencies and the error bars are the standard deviations from the mean of the averaged values.

to controls ($\sim 5 \mu\text{m}$). In a 4 g/l 37 °C model, the pore size remained nearly the same as in collagen hydrogels prior to cell culture.

2.2. 37 °C topographic 3D cellular models at 2 g/l collagen solid content: In addition to the embedded models, we prepared a set of different topographic 3D models of G-Olig2 stem cells seeded on top of collagen hydrogels. In one set of experiments, cells were seeded and induced with RA directly on top of the pre-formed 2 g/l hydrogels. In another

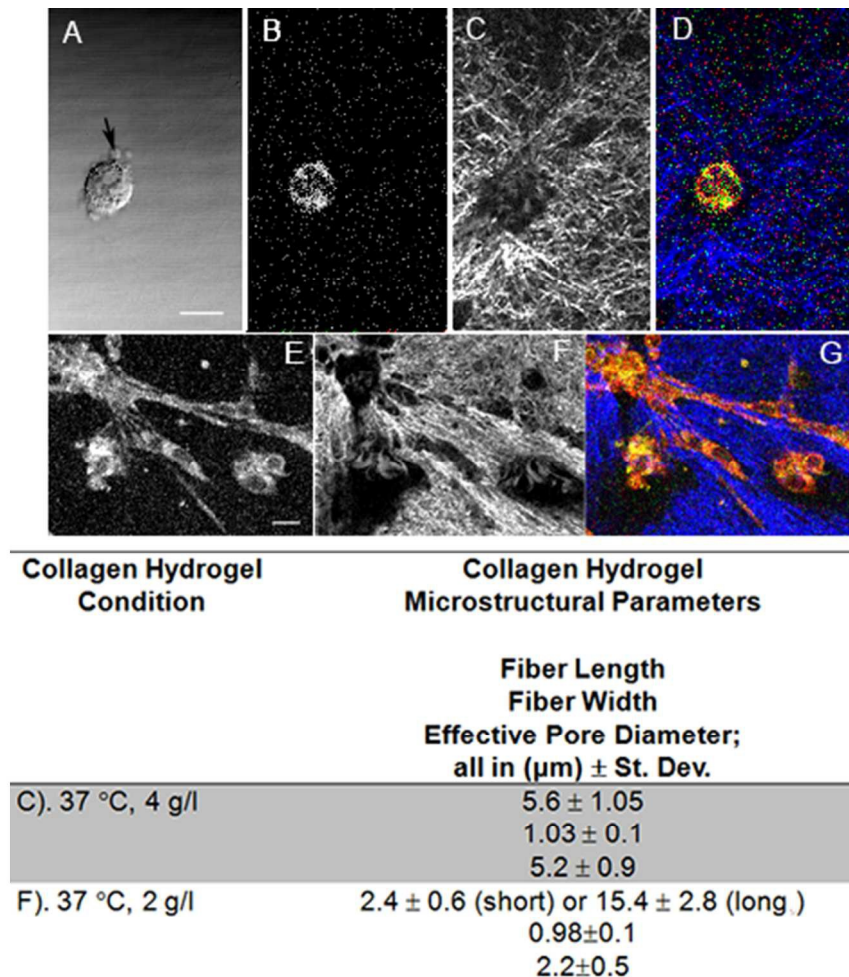


Figure 5. Multi-photon images of the 37 °C 3D encapsulated models at 4 g/l (A-D) or 2 g/l (E-G) collagen solid content. Multi-photon images were taken on day six of cell culture. (A): True-focus transmission image showing overall arrangement of embryonic stem cells. The arrow points to a $\sim 5 \mu\text{m}$ bleb routinely observed in the undifferentiated stem cell; (B)&(E): Two photon fluorescence (TPF) images of the G-Olig2 embryonic stem cells. $\lambda_{\text{ex}} = 770 \text{ nm}$. $\lambda_{\text{em}} = 390\text{--}465 \text{ nm} + 530\text{--}590$ band-pass filters; (C)&(F): Second harmonic generation (SHG) images of a surrounding collagen hydrogel. $\lambda_{\text{ex}} = 800 \text{ nm}$; (D)&(G): images in (B)&(C) are superimposed and (E) & (F) are superimposed respectively. Focusing objective is Zeiss; 40 \times water immersion; NA 0.8. Scale bar is 20 μm . Table summarizes the measured collagen hydrogels' parameters after cell culture and lists standard deviations from the mean.

1
2
3 set of experiments, cells were seeded and induced on the pre-formed 2 g/l collagen
4 hydrogels that were cross-linked separately with non-toxic reagents 0.1 M carbodiimide,
5 0.1 M carbodiimide/0.025 M NHS or 1 mM genipin. Sundararaghavan et al.³⁷ entrapped
6 L929 fibroblasts in collagen hydrogels, directly exposed them for 24 hours to culture
7 medium containing 1 mM genipin and showed that cells survive at numbers statistically
8 not different from controls that consisted of cells entrapped in collagen hydrogels with no
9 genipin added. Several other studies reported low toxicity following rinsing (extensively
10 done in our work) of the tissues cross-linked with genipin. The other chemicals that we
11 used to stabilize gels (carbodiimide (EDC) and *N*-Hydroxysuccinimide (NHS)) are not
12 considered to be cytotoxic either. We did not add any chemical directly to cells and
13 removed them prior to cell culture through rinsing.
14
15
16

17
18 ***Multiphoton imaging of collagen hydrogels' microstructure:*** After culturing stem cells
19 for five days on various collagen hydrogels we examined hydrogels' microstructure with
20 SHG imaging. The fibers within non-cross-linked 2 g/l gels became aligned (**Figure 6B**)
21 at the periphery of cellular cluster (**Figure 7A**), which started to form on the second day
22 of cell culture. Collagen fibers were absent in the area directly under where the cellular
23 cluster resided (**Figure 6B**). The rest of the collagen hydrogel was as initially prepared.
24 The lengths of collagen fibers located in the proximity of cells were heterogeneous. The
25 short fibers were similar in length to collagen fibers within control hydrogels (4.8 ± 1.1
26 μm). Long, newly induced 'fiber-like' structures were nearly 40 μm in length. The fiber
27 widths remained similar to controls ($\sim 1 \mu\text{m}$) while the effective pore sizes were slightly
28 smaller ($\sim 2 \mu\text{m}$) compared to controls ($\sim 5 \mu\text{m}$).
29
30

31 Cells aligned collagen fibers of the materials modified with EDC (**Figure 6C**) but
32 not of the materials modified with EDC/NHS (**Figure 6D**). In both EDC and EDC/NHS
33 modified materials, upon cell culture, there were short fibers similar to controls
34 ($4.8 \pm 1.1 \mu\text{m}$). However, EDC modified materials also developed longer fibers of varying
35 lengths (15 μm to 35 μm) upon cell culture. Fiber widths within EDC and EDC/NHS
36 stabilized materials were similar to controls ($\sim 1 \mu\text{m}$). The pore size for the EDC
37 stabilized materials were $\sim 5 \mu\text{m}$ and were similar to controls. In the EDC/NHS stabilized
38 materials there was almost a 2 fold reduction in the pore size after culturing cells on
39 them.
40
41

42 In the genipin stabilized 37 °C, 2 g/l models, there are some SHG generating
43 fibers that have lengths of $\sim 3 \mu\text{m}$, which is similar to what is observed in the materials
44 prior to cell culture. Fluorescent fibers ($\sim 20 \mu\text{m}$) induced upon genipin modification
45 remain nearly the same length after cell culturing. Prior to cell culture, in the genipin-
46 modified materials the width of SHG generating fibers is $\sim 1 \mu\text{m}$ while widths of
47 fluorescent fibers vary in size between 2 μm and 5 μm . After five days of culturing stem
48 cells on genipin-stabilized hydrogels, the width of SHG generating fibers remained
49 similar to that seen in the original materials while the width of fluorescent fibers reduced
50 to between 0.6 μm and 2 μm . In the collagen hydrogels prior to cell culture, the size of
51 the effective pores is $\sim 5 \mu\text{m}$ when evaluated from the SHG images and is 15 to 25 μm
52 when measured from the images that captured fluorescent fibers. The SHG signals are too
53 weak to determine effective pore sizes in collagen hydrogels after culturing stem cells on
54
55
56
57
58
59
60

them. Based on the measurements from fluorescence images the size of the effective pores does not change significantly after cell culture ($25\pm 4.5 \mu\text{m}$).

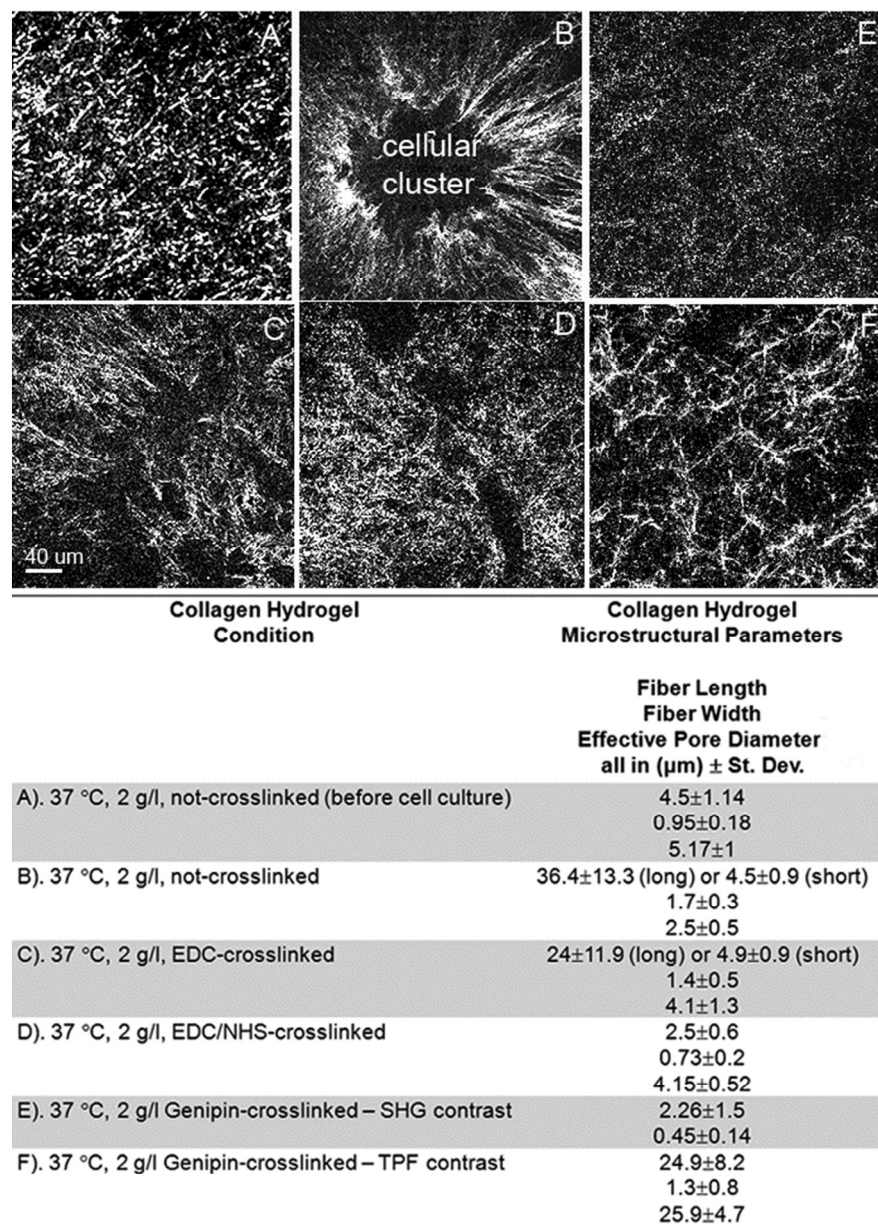


Figure 6. Multi-photon images show the microstructure of 2 g/l 37 °C collagen hydrogels before (A) and after (B-F) culturing induced G-Olig2 embryonic stem cells on top of them. (A) Second Harmonic Generation (SHG) image of non-cross-linked hydrogel prior to cell culture. (B) SHG image of non-cross-linked hydrogel after cell culture for five days. (C) SHG image of EDC-crosslinked hydrogel after cell culture for five days. (D) SHG image of EDC+NHS cross-linked hydrogel after cell culture for five days. (E) SHG image of genipin cross-linked hydrogel after cell culture for five days. (F) TPF image of genipin cross-linked hydrogel after cell culture for five days. Table under the images summarizes collagen fiber lengths, width, effective pore sizes and deviations from the mean measurements.

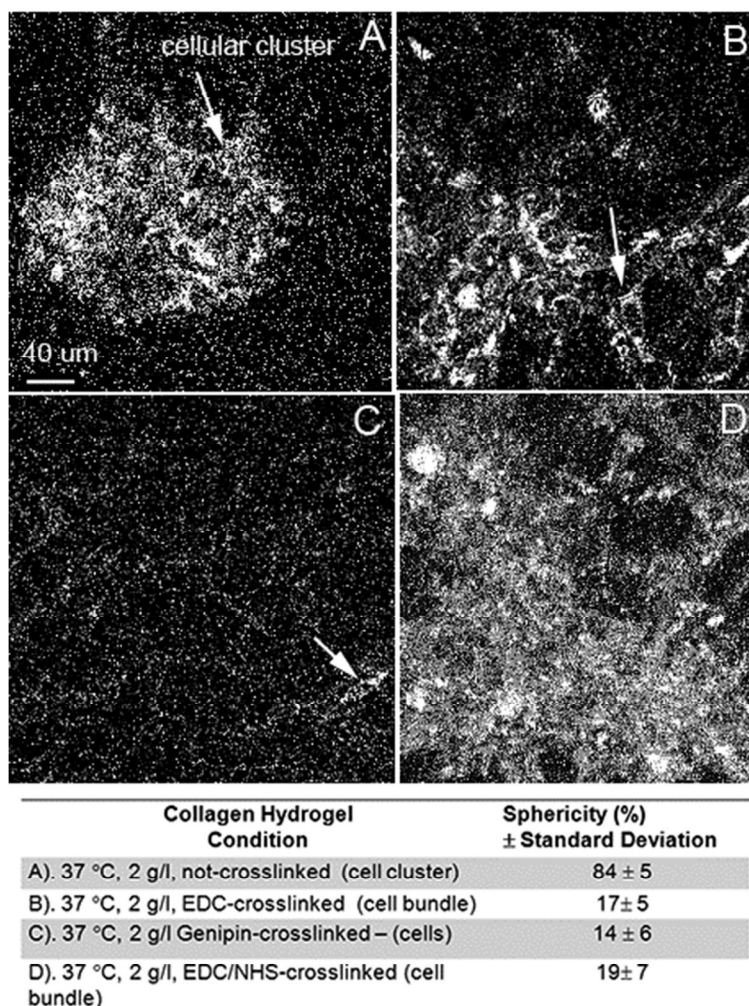


Figure 7. Two photon fluorescence images of cultured induced G-Olig2 embryonic stem cells on top of non-cross-linked (A), EDC-cross-linked (B), genipin-cross-linked (C) and EDC+NHS-cross-linked (D) 2 g/l 37 °C collagen hydrogels. $\lambda_{ex} = 770$ nm. $\lambda_{em} = 390\text{--}465$ nm + 530–590 band-pass filters. Table below summarizes single cells', cellular bundles' or cellular clusters' sphericity parameter on different hydrogels and the corresponding standard deviations of the mean.

Imaging stem cells cultured on top of collagen hydrogels.

Figure 7A shows that after culturing stem cells for five days they aggregated into clusters ($134 \mu\text{m} \pm 33 \mu\text{m}$ –bigger and $113 \mu\text{m} \pm 29 \mu\text{m}$ –smaller directions) on top of 2 g/l 37 °C collagen hydrogels that have not been cross-linked. On EDC and EDC/NHS cross-linked hydrogels materials, the stem cells scattered and formed bundles (Figure 7B,D). In the clusters, the cells were very close together, creating a 'mass' that could be separately identified (as seen in the figure) and forming actual aggregates. In the bundles the cells were loosely connected. The embryonic stem cells cultured on top of genipin-stabilized hydrogels (Figure 7C) were slender compared to those on EDC or EDC/NHS

strengthened materials and remained highly scattered. The aspects ratio results (Figure 7) indicate that the cellular clusters formed on the 2 g/l collagen hydrogels that have not been cross-linked are fairly round ($84\pm 15\%$ sphericity), while on genipin-stabilized hydrogels the dispersed cells are elongated with aspect ratio of $14\pm 5\%$.

2.3. 27 °C, 2 g/l or 4 g/l and 37 °C, 4 g/l three-dimensional topographic models:

Disaggregated collagen fibers characterized by very weak second harmonic generation (SHG) signals were detected on day five of stem cell culture that employed 27 °C self-assembled collagen hydrogels (Figure 8B, 27 °C, 2 g/l hydrogel). The SHG signals from collagen were strong and the microstructure was completely intact at the depth within hydrogels, which was naturally excluded from any contact with stem cells. As quantified from SHG images, in the topographic stem cell models prepared from 2 g/l and 4 g/l initial collagen concentrations at 27 °C self-assembly temperature (Figure 8), the fiber lengths were $\sim 20\ \mu\text{m}$, which is half of their $\sim 50\ \mu\text{m}$ length prior to cell culture (Table 2). The fiber width was reduced from $\sim 7\ \mu\text{m}$ to $\sim 4\ \mu\text{m}$ (Table 2 and Figure 8). There is 40 – 50 μm pore associated with 27 °C collagen hydrogels and it does not change upon culturing stem cells on this material.

After culturing stem cells on top of 4 g/l 37 °C hydrogels, the fiber lengths became much smaller (0.5 μm) compared to controls. The fiber widths were 0.5 μm and the effective pore sizes were not measurable in the topographic model due to low intensity of second harmonic generation (SHG) signal from disaggregated fibers.

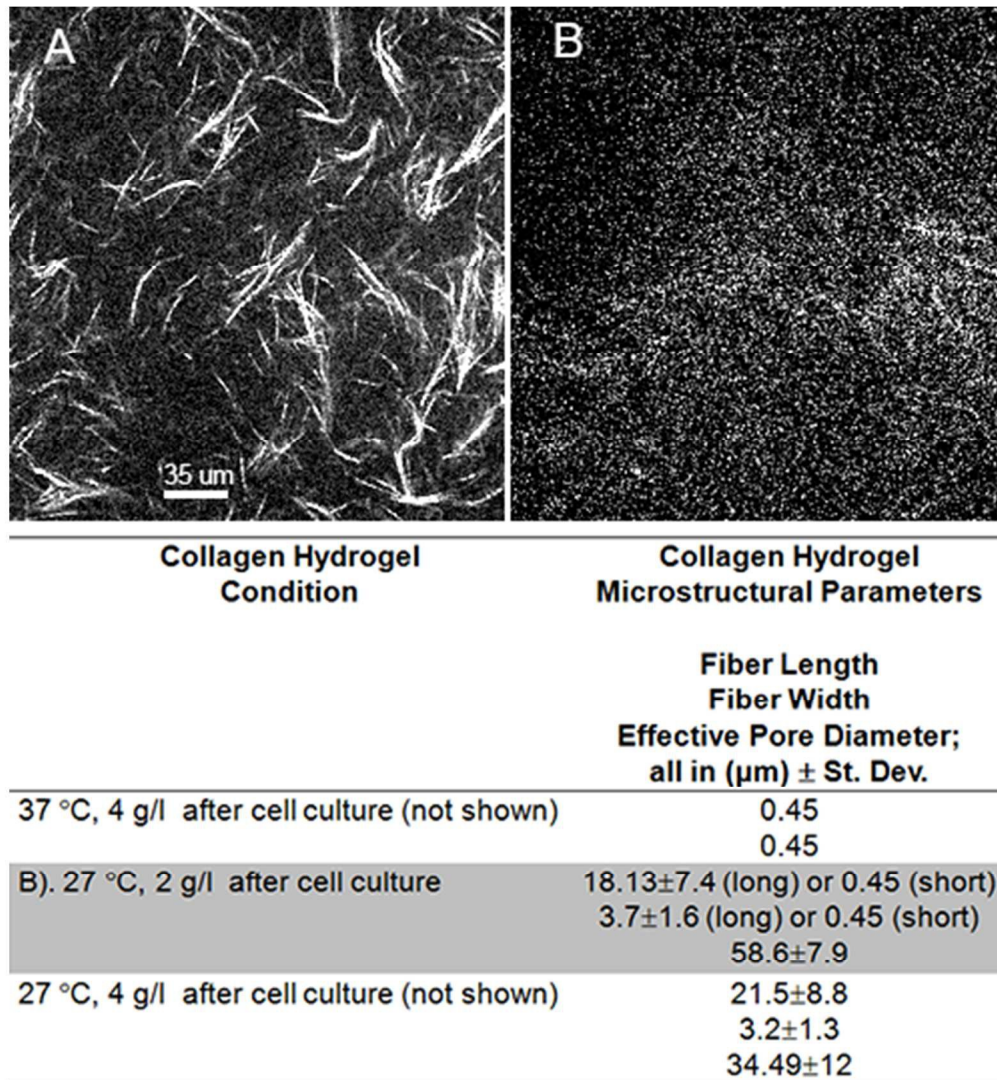
The stem cells cultured on top of 27 °C 2 g/l hydrogels, did not exhibit propensity to aggregate into round clusters as they did on 37 °C self-assembled materials prepared at the same collagen solid content. Instead, on top of 27 °C 2 g/l hydrogels cells extended and formed bundles with $20\pm 8\%$ sphericity. On the other hand, on top of 27 °C 4 g/l hydrogels, cells did not extend as much and had $88\pm 11\%$ sphericity. Similarly to 27 °C 4 g/l hydrogels, cells cultured on top of 37 °C 4 g/l collagen hydrogels remained largely not extended with $40\pm 25\%$ sphericity for those that did extend and $98\pm 11\%$ sphericity for cells that remained not extended.

Discussion

1. Advanced characterization of synthesized collagen hydrogels

1.1 Optical properties and microstructure of synthesized collagen hydrogels

To date, an understanding how physicochemical self-assembly conditions, cross-linking and degradation processes of scaffolds affect collagen formulations is limited. In hindsight, low reproducibility and predictability of the fate and behavior of cells interacting with soft materials³⁸ could be due to their incomplete characterizations as a result of a short supply of noninvasive methods. We employ spectroscopic characterization, to further follow the processes taking place during modification of collagen within hydrogels with a genipin reagent and resulting optical properties of synthesized materials. We also quantify collagen fiber and effective pore structure within hydrogels prior and during cell culture.



36 **Figure 8.** Second Harmonic Generation (SHG) images show the microstructure of 2
37 g/l 27 °C collagen hydrogels before (A) and after (B) culturing induced G-Olig2
38 embryonic stem cells on top of them. Table below the images, summarizes collagen
39 fiber lengths, width and effective pore sizes within hydrogels during the cell culture.
40 The errors shown are the standard deviations from the mean values.
41
42

43
44
45 An increase in the density of collagen triple helices aligned in a parallel way
46 within fibrils³⁹ and/or an increase in the number of fibrils' interfaces within the collagen
47 fibers,⁸ are responsible for second harmonic generation (SHG) signals from collagen
48 structures. The intra- and intermolecular cross-linking of collagen molecules by genipin
49 is expected to extend to all levels of collagen organization, including triple helices, their
50 alignment within fibrils and interfaces of collagen fibrils within fibers. The attenuation of
51 SHG signals in the genipin crosslinked collagen hydrogels is a result of this strong
52 modifying effect. Genipin was shown to form polymeric structures of 40 to 44 monomers
53 long upon its reaction with methylamine.⁴⁰ The newly formed genipin oligomeric
54 structures are what possibly additionally bridges the collagen molecules between the
55 adjacent fibrils⁴¹ within hydrogels. The carbodiimide which connects the carbonyl
56
57
58
59
60

1
2
3 containing residues of aspartic and glutamic acids and amino groups cannot bridge these
4 groups when they are located on the adjacent collagen microfibrils, which are too far
5 apart (1.3 μm to 1.7 μm).⁴¹
6
7

8 **1.2. Enzymatic degradation assay of synthesized collagen hydrogels**

9 Conventional degradation assays employ *in vitro* methods that determine
10 fractional mass loss during degradation of a polymeric biomaterial such as collagen
11 hydrogel. The methods rely on measuring dry sample weight of degraded samples and
12 comparing it with initial dry weight. This process of evaluating materials' degradation
13 removes materials from further experimentations, can lack accuracy due to a need to
14 precisely weigh increasingly small amounts of sample and is not applicable to *in vivo*
15 examinations of degrading scaffolds. Histological and immunohistochemical methods
16 that are also conventionally employed are invasive as well. They carry little information
17 regarding structural or functional status of scaffolds. Furthermore, *in vivo*, many enzymes
18 that degrade biomaterials including hydrogels would exert predominantly surface effect
19 during degradation,⁴² necessitating development of non-invasive imaging techniques
20 including fluorescent tagging⁴³ that have potential to track surface modifications by
21 enzymes. Our work outlines a non-destructive imaging method utilizing SHG and TPF
22 contrasts, to follow degradations of collagen hydrogels *in situ*. It can obtain a more
23 comprehensive level of detail regarding hydrogels' degradation patterns/kinetics, and to
24 quantify collagen fiber and effective pore structure within them during degradation. The
25 method can be applied to other soft materials with only minor modifications.
26
27
28
29
30

31 **1.3. Rheology analysis of synthesized hydrogels**

32 Collagen hydrogels exhibit viscoelastic properties that are related to their
33 composition and multiscale organization of collagen protein. The solid phase within the
34 hydrogel further interacts with liquid phase of the final preparations. To assess the
35 characteristic properties and behavior of all prepared hydrogels, we carried out dynamic
36 mechanical analysis. We determined the storage modulus – a measure of the elastic
37 energy stored (G') and the loss modulus – a measure of the energy lost through the flow
38 (G''). The ratio of G''/G' is used to evaluate viscoelasticity, since in a purely elastic
39 material, $G'' = 0$ and in a Newtonian viscous material $G' = 0$.
40
41

42 The hydrogels prepared in this study are stable over the low frequency range as
43 indicated by G' and G'' running nearly parallel. In the low frequency range, for both 2 g/l
44 and 4 g/l 37 °C hydrogels, the elastic modulus G' is significantly greater than the viscous
45 G'' modulus. On the other hand, for 2 g/l 27 °C hydrogels, G' and G'' overlap and can be
46 considered indistinguishable within the standard deviation of the measurement, indicating
47 that **it** is not a very solid gel network. In shear rheology measurements we performed, the
48 collagen fiber network and solution phases deform together. Therefore, the rheology
49 measurements on 27 °C gels could be affected by the liquid phase of collagen gel's
50 effective pores. For example, the effective pores tend to be much greater in 2 g/l 27 °C
51 assembled materials (50 $\mu\text{m} \pm 11 \mu\text{m}$) compared to 2 g/l 37 °C assembled materials (5
52 $\mu\text{m} \pm 1 \mu\text{m}$). Alternatively, the greater variability in the viscosity, G' , G'' for hydrogels
53 prepared at 27 °C could be due to 3D heterogeneity intrinsic to these materials.⁸
54
55

56 The increase in the moduli for the 2 g/l 37 °C cross-linked hydrogels correlated
57 with the degree of cross-linking: the greater was the degree of cross-linking the higher the
58
59
60

1
2
3 moduli. Genipin was the only reagent, however, that led to a sizable increase in the G'
4 elastic modulus of collagen hydrogels. All cross-linkers, however, reduced the viscous
5 part G'' of the modulus, implying that cross-linked materials are more solid-like, rigid
6 and non-flowing compared to non-cross-linked counterparts. The reductions in the
7 viscous modulus were observed in the studies that examined cross-linking of collagen
8 hydrogels with a reducing sugar glucose-6-phosphate.⁴⁴

11 **2. Characterization of the collagen hydrogel three-dimensional cellular models**

12
13
14 In this study we constructed cell-containing models while using biocompatible
15 collagen hydrogels of the micro-, nano-^{8, 18} and molecular³⁵ structure characterized prior
16 to cell culture. Previous studies utilizing phase contrast images⁴⁵ and analysis of time-
17 lapse videos of displacement of 6 μm beads trapped within collagen matrices recognized
18 that fibroblasts can translocate collagen fibrils in the collagen hydrogels prepared at low
19 collagen concentration (1 g/l) while fibrils stay stationary for the matrices prepared at
20 higher (4 g/l) collagen concentration. To our knowledge, in this work we present first
21 direct evidence of the hydrogels' microstructures that can result from collagen fiber
22 translocations.

23
24
25 Some cellular behavior described in our work that was previously documented for
26 the 3T3 fibroblasts, includes merging of cells to form tissue-like aggregates when plated
27 on soft substrates consisting of collagen coated polyacrylamide while migrating away
28 from each other and spreading on stiff substrates.⁴⁶ The stiffness of substrates was
29 7.69 ± 2.85 kPa and 2.68 ± 0.99 kPa for the stiff and soft substrates respectively based on
30 the Young's modulus obtained with Atomic Force Microscopy (AFM). Similarly, the
31 stiff substrates produced high traction forces and promoted scattering of Madin-Darby
32 canine kidney cells.⁴⁷

33
34 EDC, EDC/NHS and genipin-crosslinked 2 g/l collagen hydrogels as well as 4 g/l
35 37 °C and 2 g/l, 4 g/l 27 °C collagen hydrogels synthesized in this work are more rigid
36 compared to 2 g/l 37 °C substrates. It seems this increase in rigidity can explain the
37 scattering behavior of cultured stem cells on top of cross-linked collagen hydrogels as
38 opposed to aggregation on the non-cross-linked 2 g/l 37 °C substrates.

39
40 The viscous component G'' of the complex shear modulus is related to "internal
41 friction" and sensitive to structural morphology, heterogeneities and relaxation processes
42 of systems. It reflects the amount of energy dissipated as heat. On the other hand, the
43 storage or elastic modulus G' is interpreted as "stiffness" and most closely associated
44 with the Young's modulus. The 4 g/l 37 °C and 27 °C self-assembled gels both have
45 significantly high values of elastic modulus. It is 142 Pa for 4 g/l 37 °C self-assembled
46 gels and 122 Pa for 4 g/l 27 °C self-assembled gels. As manifested by G'', the dissipated
47 energy in these materials as well as in any non-cross-linked collagen gel, is higher than in
48 the cross-linked scaffolds. We, therefore, speculate that a combination of the higher
49 viscosity and reduction in pore size impeded cellular scattering and extension on 4 g/l 37
50 °C and 27 °C self-assembled gels.

51
52
53 In the scientific literature that addressed relationship between mechanical
54 properties of soft materials and cellular behavior, the stiffness values determined are
55 Young (or elastic) modulus obtained from various types of mechanical measurements
56 including AFM, vibrational resonance, indentation, tension, compression and rheology.⁴⁸

1
2
3
4
5
6
7
8
9
10
11
12
13
14
15
16
17
18
19
20
21
22
23
24
25
26
27
28
29
30
31
32
33
34
35
36
37
38
39
40
41
42
43
44
45
46
47
48
49
50
51
52
53
54
55
56
57
58
59
60

1
2
3
4
5
6
7
8
9
10
11
12
13
14
15
16
17
18
19
20
21
22
23
24
25
26
27
28
29
30
31
32
33
34
35
36
37
38
39
40
41
42
43
44
45
46
47
48
49
50
51
52
53
54
55
56
57
58
59
60

These measurements in many cases are not easily translated to fibrous collagen hydrogels. Additionally, in fibrous collagen hydrogels, bulk mechanical property measurements obtained by compression, rheology or in tension reflect very different elements within these systems and happen to be independent of fiber strengths.⁴⁹ For example, since collagen fibers do not rearrange upon shear loading and do not support loads as in tension, the shear elastic modulus obtained from rheological measurements is much lower than tensile elastic modulus. As additional information regarding cellular behavior on different gel-like materials of similar stiffness is emerging, it seems that a single parameter of stiffness does not provide a full scope for understanding these complex biosystems.³⁸ Material chemistry,⁵⁰ biofunctionalization,⁵¹ mechanics,⁵ and structure⁵²⁻⁵⁴ are all potentially important factors in modulating cellular behavior on/within biomaterials.^{53, 54}

Conclusions

Multiphoton microscopy (MPM) imaging that combines two-photon fluorescence (TPF) and second harmonic generation (SHG) contrasts helped to identify that for the 4 g/l 37 °C and both 2 and 4 g/l 27 °C self-assembled collagen hydrogels the stem cell extension was concomitant with collagen fibers' disaggregation near the cells.

The extension rate of stem cells on top or within 4 g/l collagen hydrogels was slower compared to 2 g/l substrates. Cultured cells modified the structure of non-cross-linked materials while the structure of cross-linked hydrogels was less affected. All cross-linkers increased rigidity of synthesized collagen gels by reducing the viscous component G'' of the complex shear modulus. The increase in collagen hydrogels' rigidity seems to explain the scattering behavior of stem cells on top of cross-linked collagen hydrogels as opposed to aggregation into clusters on the non-cross-linked 2 g/l 37 °C substrates.

MPM aided in quantifying and understanding the degradation pattern and kinetics of synthesized hydrogels with collagenase. This work provides an outline to monitor non-destructively *in situ* the outcomes of cellular culture in tissue engineering and regenerative medicine applications that utilize millimeters in thickness scattering materials.

Figure Captions

Table 1. Summary of the stem-cell models that employed 3D collagen hydrogels.

Figure 1. The experimental schematic. (A) Overview of an experimental strategy; (B) Typical one photon absorbance spectrum (left). The one photon absorbance spectrum of fresh genipin solution used to modify materials is shown for comparison. Typical two-photon fluorescence (TPF) spectra (right) of genipin modified collagen hydrogels; (C)

1
2
3
4
5
6
7
8
9
10
11
12
13
14
15
16
17
18
19
20
21
22
23
24
25
26
27
28
29
30
31
32
33
34
35
36
37
38
39
40
41
42
43
44
45
46
47
48
49
50
51
52
53
54
55
56
57
58
59
60

Second harmonic generation (SHG) images ($\lambda_{\text{ex}}/\lambda_{\text{em}} = 810 \text{ nm}/400\text{--}410 \text{ nm}$, white arrows point to the white fibers; effective pores are the black spaces between the white fibers) and two-photon fluorescence (TPF) images ($\lambda_{\text{ex}}/\lambda_{\text{em}} = 810 \text{ nm}/470\text{--}550 \text{ nm} + 570\text{--}610 \text{ nm}$) of a genipin-modified hydrogel; (D) The output mechanical properties such as storage modulus G' , loss modulus G'' and viscosity η of the prepared materials were characterized as well.

Figure 2. Quantifying genipin cross-linking reaction with collagen within hydrogels. The hydrogels were prepared at 0.3 M sodium chloride, pH 7.4, 30 mM phosphate, 37 °C polymerization temperature, 2 g/l collagen solid content. After 24-hour incubation, samples were modified for another 24 hours by 1 mM genipin solution adjusted to pH 7.4. The optical filter used to acquire SHG signals was $405\pm 5 \text{ nm}$. The spectral range of acquired TPF#1 was 470 – 550 nm. The spectral range of acquired TPF#2 was 570 – 610 nm.

Table 2. Summary of collagen hydrogel microstructural parameters and corresponding standard deviations from the mean. The hydrogels were prepared at 0.3 M sodium chloride, pH 7.4, 30 mM phosphate, 37 °C or 27 °C self-assembly temperatures and collagen solid content of 2 g/l or 4 g/l. Additionally, some hydrogels were separately cross-linked with carbodiimide (EDC), carbodiimide (EDC)/N-Hydroxysuccinimide (NHS) or genipin.

Figure 3. The effect of collagen hydrogels' digestion by a topically applied collagenase solution. Typical *in situ* degradation kinetics plot for 2 g/l 37 °C polymerized non-cross-linked hydrogel (Left). Second Harmonic Generation (SHG) images collected with 20× Olympus objective show microstructure of a collagen hydrogel immediately after collagenase solution was added (A) and 25 min later (B). Tables (Bottom) summarize the porosity of collagen hydrogels detected in real time during degradation with collagenase.

Figure 4. Storage moduli G' for collagen hydrogels prepared at different collagen solid content and self-assembly temperatures (A); Loss moduli G'' for collagen hydrogels prepared at different collagen solid content and polymerization temperatures (B); Relative storage moduli G' for collagen hydrogels cross-linked with EDC, EDC/NHS and genipin reagents (C); Relative loss moduli G'' for collagen hydrogels cross-linked with EDC, EDC/NHS and genipin reagents (D). For non-cross-linked gels, the data plotted is for 0.1 Hz frequency and error bars reflect the standard deviations from the mean measured values. For cross-linked gels, the data plotted is an average for 0.1 – 1 Hz frequencies and the error bars are the standard deviations from the mean of the averaged values.

Figure 5. Multi-photon images of the 37 °C 3D encapsulated models at 4 g/l (A-D) or 2 g/l (E-G) collagen solid content. Multi-photon images were taken on day six of cell culture. (A): True-focus transmission image showing overall arrangement of embryonic stem cells. The arrow points to a $\sim 5 \mu\text{m}$ bleb routinely observed in the undifferentiated stem cell; (B)&(E): Two photon fluorescence (TPF) images of the G-Olig2 embryonic stem cells. $\lambda_{\text{ex}} = 770 \text{ nm}$. $\lambda_{\text{em}} = 390\text{--}465 \text{ nm} + 530\text{--}590 \text{ band-pass filters}$; (C)&(F):

1
2
3
4
5
6
7
8
9
10
11
12
13
14
15
16
17
18
19
20
21
22
23
24
25
26
27
28
29
30
31
32
33
34
35
36
37
38
39
40
41
42
43
44
45
46
47
48
49
50
51
52
53
54
55
56
57
58
59
60

Second harmonic generation (SHG) images of a surrounding collagen hydrogel. $\lambda_{\text{ex}} = 800$ nm; (D)&(G): images in (B)&(C) are superimposed and (E) & (F) are superimposed respectively. Focusing objective is Zeiss; 40 \times water immersion; NA 0.8. Scale bar is 20 μm . Table summarizes the measured collagen hydrogels' parameters after cell culture and lists standard deviations from the mean.

Figure 6. Multi-photon images show the microstructure of 2 g/l 37 $^{\circ}\text{C}$ collagen hydrogels before (A) and after (B-F) culturing induced G-Olig2 embryonic stem cells on top of them. (A) Second Harmonic Generation (SHG) image of non-cross-linked hydrogel prior to cell culture. (B) SHG image of non-cross-linked hydrogel after cell culture for five days. (C) SHG image of EDC-crosslinked hydrogel after cell culture for five days. (D) SHG image of EDC+NHS cross-linked hydrogel after cell culture for five days. (E) SHG image of genipin cross-linked hydrogel after cell culture for five days. (F) TPF image of genipin cross-linked hydrogel after cell culture for five days. Table under the images summarizes collagen fiber lengths, width, effective pore sizes and deviations from the mean measurements.

Figure 7. Two photon fluorescence images of cultured induced G-Olig2 embryonic stem cells on top of non-cross-linked (A), EDC-cross-linked (B), genipin-cross-linked (C) and EDC+NHS-cross-linked (D) 2 g/l 37 $^{\circ}\text{C}$ collagen hydrogels. $\lambda_{\text{ex}} = 770$ nm. $\lambda_{\text{em}} = 390\text{--}465$ nm + 530–590 band-pass filters. Table below summarizes single cells', cellular bundles' or cellular clusters' sphericity parameter on different hydrogels and the corresponding standard deviations of the mean.

Figure 8. Second Harmonic Generation (SHG) images show the microstructure of 2 g/l 27 $^{\circ}\text{C}$ collagen hydrogels before (A) and after (B) culturing induced G-Olig2 embryonic stem cells on top of them. Table below the images, summarizes collagen fiber lengths, width and effective pore sizes within hydrogels during the cell culture. The errors shown are the standard deviations from the mean values.

Acknowledgements

The work was funded in part by National Science Foundation (BRIGE EEC-0927297 and CAREER CBET-0847070, J.G.L.), UC Faculty Regents Fellowship, (J.G.L.), UC Riverside startup research funds (J.G.L.) and UC Riverside Dissertation Fellowship (Y.J.H). We thank Prof. Bruce J. Tromberg for access to a Zeiss LSM 510 NLO Meta microscopy system (S10-RR022612) at UC Irvine supported under the NIH Biomedical Technology Resource, Grant No. P41-RR01192 and a UC BSAS Grant (J.G.L). We also thank Dr. Chung-ho Sun for the valuable initial discussions regarding work with G-Olig2 embryonic stem cell line and its initial expansion. We thank a UCR undergraduate bioengineering student Akhila Denduluri for help with processing and organizing a multitude of multi-photon microscopy images collected as part of this study.

References

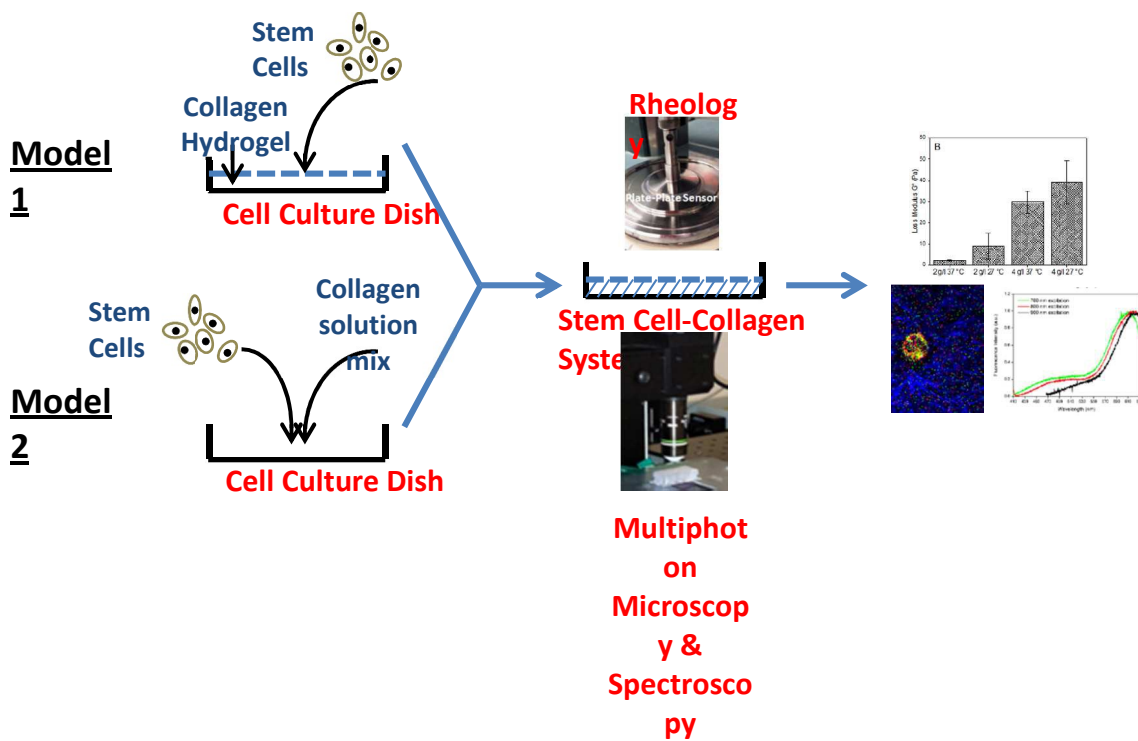
1. B. E. Reubinoff, M. F. Pera, C. Y. Fong, A. Trounson and A. Bongso, *Nat. Biotechnol.*, 2000, **18**, 399-404.

2. D. Sengupta and S. C. Heilshorn, *Tissue Eng. Part B Rev.*, 2010, **16**, 285-294.
3. M. M. Stevens and J. H. George, *Science*, 2005, **310**, 1135-1138.
4. G. C. Reilly and A. J. Engler, *J. Biomech.*, 2010, **43**, 55-62.
5. A. J. Engler, S. Sen, H. L. Sweeney and D. E. Discher, *Cell*, 2006, **126**.
6. V. L. Cross, Y. Zheng, C. N. Won, S. S. Verbridge, B. A. Sutermeister, L. J. Bonassar, C. Fischbach and A. D. Stroock, *Biomaterials*, 2010, **31**, 8596-8607.
7. X. Lang and J. G. Lyubovitsky, *Anal. Meth.*, 2015, **7**, 1680 - 1690.
8. Y. Hwang and J. G. Lyubovitsky, *Anal. Meth.*, 2011, **3**, 529-536.
9. R. J. J. Pelham and Y. Wang, *Proc. Natl. Acad. Sci. USA*, 1997, **94**, 13661-13665.
10. A. Pathak and S. Kumar, *Integr. Biol.*, 2011, **3**, 267-278.
11. G. P. Raeber, M. P. Lutolf and J. A. Hubbell, *Biophys. J.*, 2005, **89**, 1374-1388.
12. A. Meshkinpour, P. Ghasri, K. Pope, J. G. Lyubovitsky, J. Risteli, T. B. Krasieva and K. M. Kelly, *Lasers in Surg. Med.*, 2005, **37** 343-349.
13. J. G. Lyubovitsky, T. B. Krasieva, J. A. Spencer, B. Andersen and B. J. Tromberg, *J. Biomed. Opt.*, 2006, **11**, 014013.
14. J. G. Lyubovitsky, X. Xu, T. B. Krasieva, B. Andersen and B. J. Tromberg, *J. Biomed. Opt.*, 2007, **12**, 044003
15. J. G. Lyubovitsky, X. Xu, C. Sun, B. Andersen, T. B. Krasieva and B. J. Tromberg, *Proc. SPIE* 2008, **6859**, 1-9
16. B. R. Masters and P. T. So *Handbook of Biomedical Nonlinear Optical Microscopy*; Oxford University Press: New York, 2008.
17. Y. Hwang, J. Granelli, M. Tirumalasetty and J. G. Lyubovitsky, *Proc. SPIE* 2013, **8587**, 858725
18. Y. Hwang, J. Granelli and J. G. Lyubovitsky, *Appl. Mater. Interfaces* 2011, **4**, 261-267.
19. Y. Hwang, J. Granelli and J. G. Lyubovitsky, *Anal. Chem.*, 2011, **83**, 200-206.
20. Y. Hwang, N. Kolletis, M. Yang, E. Sanchez, C. Sun, E. R. Gillard, B. J. Tromberg, T. B. Krasieva and J. G. Lyubovitsky, *Photochem. Photobiol.*, 2011, **87**, 408-417
21. Y. Hwang, J. Larsen, T. Krasieva and J. G. Lyubovitsky, *Appl. Mater. Interfaces* 2011, **3**, 2579-2584
22. C. B. Raub, V. Suresh, T. B. Krasieva, J. G. Lyubovitsky, J. D. Mih, A. J. Putnam, B. J. Tromberg and S. C. George, *Biophys. J.*, 2007, **92**, 2212-2222.
23. X. Lang, M. Spousta and J. G. Lyubovitsky, *Proc. SPIE* 2015, **9329**, doi:10.1117/1112.2080559.
24. N. I. zur Nieden, C. C. Turgman, X. Lang, J. M. Larsen, J. Granelli, Y. Hwang and J. G. Lyubovitsky, *Appl. Mater. Interfaces*, 2015, **7**, 10599-10605.
25. S. Dhall, D. C. Do, M. Garcia, J. Kim, S. Mirebrahim, J. Lyubovitsky, S. Lonardi, E. A. Nothnagel, N. L. Schiller and M. Martins-Green, *J. Diabetes Res.*, 2014, **2014**, Article ID 562625.
26. S. Dhall, D. C. Do, M. Garcia, D. S. Wijesinghe, A. P. Brandon, J. Kim, A. Sanchez, J. Lyubovitsky, S. Gallagher, E. A. Nothnagel, C. E. Chalfant, R. P. Patel, N. Schiller and M. Martins-Green, *PLoS ONE*, 2014, **9**, e109848.
27. M. Martins-Green, M. Frankos, N. Adhami, M. Valdez, B. Goodwin, J. Lyubovitsky, S. Dhall, M. Garcia, I. Egiebor, B. Martinez, P. Jacob III, C. Havel, L. Yu and M. Curras-Collazo, *PLoS ONE* 2014, **9**, e8639

- 1
 - 2
 - 3
 - 4
 - 5
 - 6
 - 7
 - 8
 - 9
 - 10
 - 11
 - 12
 - 13
 - 14
 - 15
 - 16
 - 17
 - 18
 - 19
 - 20
 - 21
 - 22
 - 23
 - 24
 - 25
 - 26
 - 27
 - 28
 - 29
 - 30
 - 31
 - 32
 - 33
 - 34
 - 35
 - 36
 - 37
 - 38
 - 39
 - 40
 - 41
 - 42
 - 43
 - 44
 - 45
 - 46
 - 47
 - 48
 - 49
 - 50
 - 51
 - 52
 - 53
 - 54
 - 55
 - 56
 - 57
 - 58
 - 59
 - 60
28. M. L. Petreaca, S. Dhall, A. Serafino, D. Do, D. McLelland, J. G. Lyubovitsky, N. Schiller and M. M. Martins-Green, *Wound Repair and Regeneration*, 2012, **20**, 353-366.
29. H. Xian, E. McNichols, A. St.Clair and D. I. Gottlieb, *Stem Cells*, 2003, **21**, 41-49.
30. G. Bain, W. J. Ray, M. Yao and D. I. Gottlieb, *Biochem. Biophys. Res. Commun.* , 1996, **223**, 691-694.
31. P. Jiang, V. Selvaraj and W. Deng, *J. Vis. Exp.* , 2010, **19**, 1960.
32. E. M. V. Jones-Villeneuve, M. A. Rudnicki, J. F. Harris and M. W. McBurney, *Mol. Cell Biol.* , 1983, **3**, 2271-2279.
33. Y. Okada, T. Shimazaki, G. Sobue and H. Okano, *Dev. Biol.*, 2004, **275**, 124-142.
34. S. Fujikawa, Y. Fukui, K. Koga and J. Kumada, *J. Ferment. Technol.*, 1987, **65**, 419-424.
35. Y. Hwang and J. G. Lyubovitsky, *Biopolymers*, 2013, **99**, 349-356.
36. L. J. Kaufman and S. Motte, *Biopolymers*, 2012, **99**, 35-46.
37. H. G. Sundararaghavan, G. A. Monteiro, N. A. Lapin, Y. J. Chabal, J. R. Miksan and D. I. Shreiber, *J. Biomed. Mater. Res., Part A*, 2008, **87**, 308-320.
38. A. M. Schaap-Oziemlak, P. T. Kuhn, T. G. van Kooten and P. van Rijn, *RSC Advances*, 2014, **4**, 53307-53320.
39. S. Bancelin, C. Aime, I. Gusachenko, L. Kowalczyk, G. Latour, T. Coradin and M.-C. Schanne-Klein, *Nat. Commun.*, 2014, **5**.
40. R. Touyama, Y. Takeda, K. Inoue, I. Kawamura, M. Yatsuzuka, T. Ikumoto, T. Shingu, T. Yokoi and H. Inouye, *Chem. Pharm. Bull.* , 1994, **42**, 668-673.
41. H. Sung, W. Chang, C. Ma and M. Lee, *J. Biomed. Mater. Res.* , 2003, **64A**, 427-438.
42. B. D. Ratner, A. S. Hoffman, F. J. Schoen and J. E. Lemons, Eds. *Biomaterials Science: An Introduction to Materials in Medicine*, 2013.
43. N. Artzi, N. Oliva, C. Puron, S. Shitreet, S. Artzi, A. bon Ramos, A. Groothuis, G. Sahagian and E. R. Edelman, *Nat. Mater.*, 2011, **10**, 704-709.
44. M. E. Francis-Sedlak, S. Uriel, J. C. Larson, H. P. Greisler, D. C. Venerus and E. M. Brey, *Biomaterials* 2009, **30** 1851-1856.
45. M. Miron-Mendoza, J. Seemann and F. Grinnell, *Biomaterials* 2010, **31**, 6425-6435.
46. W. Guo, M. T. Frey, N. A. Burnham and Y. Wang, *Biophys. J.*, 2006, **90**, 2213-2220.
47. J. de Rooij, A. Kerstens, G. Danuser, M. A. Schwartz and C. M. Waterman-Storer, *J. Cell Biol.*, 2005, **171**, 153-164.
48. I. Levental, P. C. George and P. A. Janmey, *Soft Matter*, 2006, **2**, 1-9.
49. J. A. Pederson and M. A. Swartz, *Ann. Biomed. Eng.*, 2005, **33**, 1469-1490.
50. D. S. W. Benoit, M. P. Schwartz, A. R. Durney and K. S. Anseth, *Nat. Mater.* , 2008, **7**, 816-823.
51. T. A. Petrie, J. E. Raynor, D. W. Dumbauld, T. T. Lee, S. Jagtap, K. L. Templeman, D. M. Collard and A. J. Garcia, *Sci. Transl. Med.*, 2010, **2**, 45ra60.
52. M. J. Dalby, N. Gadegaard, R. Tare, A. Andar, M. O. Riehle, P. Herzyk, C. D. W. Wilkinson and R. O. C. Oreffo, *Nat. Mater.*, 2007, **6**, 997-1003.

- 1
2
3
4
5
6
7
8
9
10
11
12
13
14
15
16
17
18
19
20
21
22
23
24
25
26
27
28
29
30
31
32
33
34
35
36
37
38
39
40
41
42
43
44
45
46
47
48
49
50
51
52
53
54
55
56
57
58
59
60
53. G. Kumar, C. K. Tison, K. Chatterjee, P. S. Pine, J. H. McDaniel, M. L. Salit, M. F. Young and C. G. J. Simon, *Biomaterials*, **2011**, **32**, 9188-9196.
54. G. Kumar, M. S. Waters, T. M. Farooque, M. F. Young and C. G. Simon Jr., *Biomaterials*, 2012, **33**, 4022-4030.

Table of Content (TOC) Entry



Imaging discovers implications for impaired collagen and other biomaterials function during culturing embryonic stem cells in and on them